Nonlinear Processes in Geophysics (1994) 1: 156 - 167

Nonlinear Processes in Geophysics

Bounded cascade clouds: albedo and effective thickness

R.F. Cahalan

Goddard Laboratory for Atmospheres, NASA-Goddard Space Flight Center, Greenbelt, MD 20771, USA

Received 3 December 1993 - Accepted 12 May 1994 - Communicated by S. Lovejoy

Abstract. If climate models produced clouds having liquid water amounts close to those observed, they would compute a mean albedo that is often much too large, due to the treatment of clouds as plane-parallel. An approximate lower-bound for this "plane-parallel albedo bias" may be obtained from a fractal model having a range of optical thicknesses similar to those observed in marine stratocumulus, since they are more nearly plane-parallel than most other cloud types. We review and extend results from a model which produces a distribution of liquid water path having a lognormal-like probability density and a power-law wavenumber spectrum, with parameters determined by stratocumulus observations. As the spectral exponent approaches -1, the simulated cloud approaches a well-known multifractal, referred to as the "singular model", but when the exponent is -5/3, similar to what is observed, the cloud exhibits qualitatively different scaling properties, the so-called "bounded model". The mean albedo for bounded cascade clouds is a function of a fractal parameter, $0 < f < 1$, as well as the usual plane-parallel parameters such as single scattering albedo, asymmetry, solar zenith angle, and mean vertical optical thickness. A simple expression is derived to determine f from the variance of the logarithm of the vertically-integrated liquid water. The albedo is shown to be approximated well by the plane-parallel albedo of a cloud having an "effective" vertical optical thickness, smaller than the mean thickness by a factor $\chi(f)$, which is given as an analytic function of f. California stratocumulus have a mean fractal parameter $f \approx 0.5$, relative albedo bias of 15%, and an effective thickness 30% smaller than the mean thickness ($\chi \approx 0.7$). For typical observed values of mean liquid water and f, the effective thickness approximation gives a plane-parallel albedo within 3% of the mean albedo.

1 Introduction

The large-scale terrestrial climate is well-known to be sensitive to small changes in the average albedo of the earth-atmosphere system. Sensitivity estimates vary, but typically a 10% decrease in global albedo, with all other quantities held fixed, increases the global mean equilibrium surface temperature by 5°C, similar to the warming since the last ice age, or that expected from a doubling of CO_2. [See, for example, Cahalan and Wiscombe, 1993.] Yet not only is the global albedo not known to 10% accuracy, but current global climate models often do not predict the albedo in each gridbox from realistic liquid water values; they simply reduce the liquid until plane-parallel radiative computations produce what are believed to be typical observed albedos. Harshvardhan and Randall (1985) have estimated that globally this requires a factor of three reduction in cloud liquid. The inability of the models to compute the albedo is due to their inability to predict the microphysical and macrophysical properties of cloud liquid water within each gridbox, and their reliance on plane-parallel radiative codes. As Stephens (1985) has emphasized, the mean albedo of each gridbox depends not only on the mean properties of the clouds within each box, but also upon the variability of the clouds, which involves not only the fractional area covered by clouds, but also the cloud structure itself. As climate models are now beginning to carry liquid water as a prognostic variable (e.g. Sundqvist et al., 1989), it is important to treat cloud radiation and cloud hydrology consistently, which requires that cloud parameterizations become dependent on the fractal structure of clouds. Radiative properties of singular multifractal clouds have been previously studied (e.g. Cahalan, 1989; Lovejoy et al., 1990; Gabriel et al., 1990; Davis et al., 1990). Here we shall show how the radiative properties of relatively thin boundary-layer clouds, and specifically the area-average albedo, depend on their fractal structure.

The dependence of average albedo on cloud structure has been found to be especially important in the case of marine stratocumulus, a major contributor to net cloud radiative forcing. Computations based on observations of California stratocumulus during the First International Satellite Cloud Climatology Regional Experiment (FIRE) have shown that stratocumulus have significant fractal structure, and that this "within-cloud" structure can have a greater impact on average albedo than cloud fraction (Cahalan and Snider, 1989; Cahalan et al, 1994a and 1994b). These studies employed a "bounded cascade" model to distribute the cloud liquid, with parameters c and f adjusted to fit the scaling exponent of the power spectrum of liquid water path (W), $\alpha(c) \approx 5/3$, and the standard deviation of $\log_{10}$ (W), $\sigma(f,c)$. In order to isolate the effects of horizontal liquid water variations on cloud albedo, the usual microphysical parameters were assumed homogeneous, as was the geometrical cloud thickness. In order to simplify comparison with plane-parallel clouds, the area-averaged vertical optical depth was kept fixed at each step of the cascade. The albedo bias was found as an analytic function of the fractal parameters, f and c, as well as the mean vertical optical thickness, τ_v, and sun angle, θ_o. For the diurnal mean of the values observed in FIRE ($f \approx 0.5$, $c \approx 0.8$, $\tau_v \approx 15$, and $\theta_o \approx 60°$) the absolute bias is approximately 0.09, or 15% of the plane-parallel albedo of 0.69.

This purpose of this paper is to show how these results for the mean albedo of bounded cascade clouds, derived in the references cited above, may be applied to parameterizing the albedo of such clouds in terms of the plane-parallel albedo of a cloud having an "effective optical thickness" which is reduced from the mean thickness by a factor $\chi(f)$ which depends only on the fractal parameters f and c, or equivalently α and σ, and not on the mean cloud properties. This "effective thickness approximation" (ETA) is a special case of the so-called "independent pixel approximation" (IPA) which neglects net horizontal photon transport. Here we determine the accuracy of this approximation for cloud parameters typical of marine stratocumulus. In addition, some previous analytic results for bounded cascades are generalized and simplified in two appendices.

In the following, we first define some terms in Section 2. Then Section 3 shows that the IPA provides estimates of the plane-parallel albedo bias accurate to about 1% for the bounded cascade, and Section 4 applies the IPA to show that the total absolute bias reaches a maximum of about 0.10 during the morning hours, when the cloud fraction is nearly 100%. These two sections are primarily summaries of results from Cahalan et al. (1994a) and Cahalan et al. (1994b), although there a 1D cascade was employed, while a here a 2D case is shown. Section 5 gives our main result, that under certain commonly-observed conditions the albedo is approximately the plane-parallel albedo at a reduced "effective optical thickness", $\tau_{eff} \equiv \chi * \tau_v$, where the reduction factor χ increases with f, and is independent of the mean vertical optical depth. The accuracy of this approximation is given as a function of both f and the mean thickness. The results are summarized and their limitations briefly discussed in Section 6. Appendix A shows that all moments of a bounded cascade may be obtained from the second moment as a function of f. This generalizes expressions for the second and third moments given in Cahalan et al. (1994a), and allows the lognormal behavior in the singular limit to be explicitly exhibited. Appendix B gives expressions for χ and σ as power series in f with coefficients depending on c, and provides rational functions of f accurate for the case of a 5/3 spectrum.

2 Definitions

Currently many general circulation models (GCMs) do not predict cloud liquid water in each gridbox, but attempt to diagnose it from other quantities. The cloud albedo is also often not predicted, but prescribed independently of the hydrological cycle. However, efforts are now underway to improve this situation (e.g. Sundqvist et al., 1989), so that simulated clouds can respond more realistically to climate change. The hope is that average cloud liquid in each gridbox will be accurately predicted, and that the resulting cloud albedo will be correctly computed from this, and other average cloud parameters. It is important to recognize, however, that *mean cloud parameters are insufficient* to compute the mean albedo. The mean albedo also depends, at a minimum, on the deviations of the liquid water from the mean, or more appropriately, on scaling exponents such as α, and on σ and higher moments of the *logarithm of the liquid water*, as we demonstrate in this paper using the bounded cascade model. To clarify the discussion, we first introduce some definitions.

The schematic in Fig.1 shows three approaches to distributing a prescribed amount of liquid water in a GCM gridbox. In (a) it is uniform over the whole area, and thus the albedo may be computed from plane-parallel theory, and depends only on the *average* optical thickness, effective particle radius, and so on. In (b) the cloud is assumed to cover only a fraction of the area, is somewhat thicker in order to contain the same total liquid, but is still assumed to be uniform on that so-called "cloud fraction". In this case the mean albedo of the gridbox is assumed to equal the weighted average of a "cloud albedo" and a "clear-sky" albedo. Finally, in (c) the cloud covers the same cloud fraction as in (b), with the same mean parameters, but is assumed to have a non-uniform structure which depends on one or more "fractal parameters". The cloud fraction and the fractal parameters are assumed to depend on geographic region, season, and time of day.

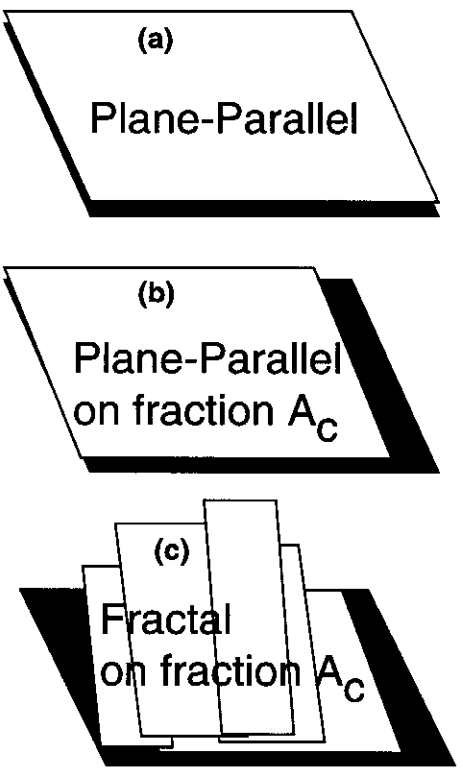

Fig. 1. Schematic showing three approaches to distributing the cloud liquid water in a GCM gridbox. In the top figure, the cloud has plane-parallel geometry, with cloud parameters such as vertical optical thickness, τ_v, uniform over the whole gridbox. In the middle figure, the parameters are uniform over a fraction A_c of the gridbox, with the same values as above, except that cloud vertical optical thickness increases to τ_v/A_c, thus preserving the total liquid, while the cloud thickness is zero on the remaining fraction $1-A_c$. In the bottom figure one has a fractal distribution of cloud parameters over the fraction A_c, with the same mean values as in the middle, and an identical clear fraction $1-A_c$.

As a measure of the impact of cloud fraction and fractal parameters on the average albedo, we define the "absolute plane-parallel albedo bias", ΔR_{pp}, as the mean albedo computed in case (a) minus that in case (c). This may be expressed symbolically as:

$$\Delta R_{pp} = R_{pp} - (A_c R_f + (1 - A_c) R_s), \tag{1}$$

where R_{pp} is the plane-parallel reflectivity, R_f is the mean reflectivity of the fractal cloud, R_s is the mean clear-sky reflectivity, and the same total liquid water is used in both cases. The *relative* plane-parallel albedo bias is the plane-parallel bias divided by R_{pp}. To avoid confusion, the absolute bias is always given as a fraction, while the relative bias is given in percent. Since the simple uniform cloud fraction model shown in Fig.1b is currently widely employed, it is convenient to split the total plane-parallel bias into the difference between (a) and (b), plus the difference between (b) and (c). Symbolically:

$$\begin{aligned} \Delta R_{pp} \;=\; & [R_{pp} - (A_c R_{pp} + (1 - A_c) R_s)] + \\ & [(A_c R_{pp} + (1 - A_c) R_s) - \\ & (A_c R_f + (1 - A_c) R_s)]. \end{aligned} \tag{2}$$

The first difference represents the bias due only to the reduction in cloud fraction from unity to A_c, and the corresponding increase in thickness, with no change in the plane-parallel assumption; the second difference is the *additional* bias due only to the within-cloud fractal structure, and again the same total liquid is employed in all cases. This section and the following considers the case of overcast clouds, having $A_c = 1$, so that the total bias depends only on the fractal parameter. Then Section 4 considers the case in which both the cloud fraction and the fractal parameter follow the diurnal variations observed in California stratocumulus. As we shall see, the $A_c = 1$ case produces the largest total bias, because of the sensitivity of the bias to the fractal structure, and the observed fact that in California stratocumulus the overcast cases have the greatest within-cloud variability.

In order to generate a bounded cascade cloud, we begin with a uniform cloud having a liquid water path of e.g. $W = 100$ g/m^2, and corresponding vertical optical thickness of e.g. $\tau_v = 15$ (i.e. 10 μm effective drop size). We assume large but finite horizontal optical thicknesses in both horizontal directions, say $\tau_v = 1500$. This uniform distribution is now made non-uniform by a bounded multiplicative cascade process, in which the cloud is successively subdivided into smaller parts, and successively smaller fractions of liquid water are transferred among these parts, without changing the total. [If the fractions were kept the same at each step, the resulting distribution would be singular, and the power spectrum would have more small-scale variability than is observed in marine stratocumulus clouds.]

Table 1. Parameters for bounded cascade clouds

Parameter	Symbol	Typical Value
single-scattering albedo	ω_0	1
asymmetry	g	0.85
liquid water path	W	100 g/m^2
vertical optical thickness	τ_v	15
effective optical thickness	τ_{eff}	10
solar zenith angle	θ_o	60°
scaling parameter	c	0.8
variance parameter	f	0.5
power spectral exponent	α	5/3
std. dev. of $\log_{10}(W)$	σ	0.4
reduction factor	χ	0.7

We first describe a one-dimensional (1D) bounded cascade, and we shall consider the simplest subdivision process: Divide the cloud in half along a north-south line. Flip a coin to select one half, and transfer a fraction, say $f_0 = f = 0.5$ from that half to the other one. The process is then iterated as follows: Each of the two halves is divided in half the same way, two coins are flipped to select one quarter from each of the two pairs, and a smaller fraction $f_1 = f * c$, with say $c = 0.8$, so that $f_1 = 0.4$, is transferred from each chosen quarter to the other one. The resulting four quarters are in turn divided in half, four coins are flipped, and a fraction $f_2 = f_1 * c = 0.32$ is transferred within the four pairs of eighths, and so on. The resulting distribution of liquid water path has a power spectrum behaving as $k^{-\alpha}$, where $\alpha \approx 5/3$ when $c = 2^{-1/3} \approx 0.8$, as observed (Cahalan and Snider, 1989), and an approximately log-normal probability distribution, with the standard deviation of $\log_{10}(W) \equiv \sigma(f) \approx 0.39$ when $f = 0.5$, as is also observed (Cahalan et al., 1994.)

A two-dimensional (2D) bounded cascade begins with the same initial cloud, which is then divided into quarters along both north-south and east-west lines, and liquid water fractions are then transferred among the quarters. Our transfer method is as follows: The four quarters are divided into two pairs, aligned either north-south, east-west or diagonally, with equal probability for each of the three possible ways. One of the pairs is selected by a coin toss, and a fraction $f_0 = f = 0.5$ is transferred within that pair, with either direction equally likely, while a fraction f_0' is transferred within the other pair. For simplicity, we also take $f_0' = f$. The process is then repeated by quartering each quarter, transferring $f_1 = 0.8 * f$, and so on. The set of optical depth values thus generated at steps 1, 2, 3, ..., N in the 2D cascade are identical to those generated at the same steps in the 1D cascade, except that each value appears twice in the first step, and 2^N times in the Nth step. The one-point probability distribution function of W and τ_v is identical in both 1D and 2D.

Table 1 summarizes the symbols and typical values of parameters in the bounded cascade cloud model. In addition to the bounded cascade, two additional assumptions are being made here. One is that the effective droplet radius is uniformly equal to 10 μm, so that the vertical optical thickness of each part of the cloud is linear in the liquid water:

$$\tau = 0.15\,W. \tag{3}$$

Second, we employ the "independent pixel approximation", which means that the reflectivity of each cloud pixel is assumed to depend only on its optical depth, $R = R(\tau)$, and not the optical depth of neighboring pixels. This is a strong assumption, and will be justified for the bounded model in the following section.

3 Independent Pixel Approximation

The grayscale map in Fig. 2a shows the reflectivity of $(64)^2$ cloud cells as computed by Monte Carlo methods for a cloud generated by 6 cascade steps of a 2D bounded cascade with mean vertical optical thickness $\tau_v = 16$, $\theta_o = 60°$, and fractal parameter $f = 0.5$. If there were no horizontal photon transport, the reflectivity of each of the $2^{12} = 4096$ cloud pixels would simply be determined by independent plane-parallel computations. The local differences between this "independent pixel approximation" (IPA) and the Monte Carlo reflectivities are shown by the grayscale map in Fig. 2b. The brighter areas of negative bias occur where the IPA underestimates the reflectivity of an optically thick region which lies on the sunward side of immediately adjacent thin regions and has an enhanced brightness due to photons escaping from those thin regions. Conversely, the darker positive regions occur where the IPA overestimates the brightness of a thin region which lies downstream of an adjacent thick region. [Recall that the cloud has constant geometric thickness everywhere, so that the horizontal photon leakage is not simple geometrical shadowing. It occurs *within* the cloud.] These local errors in the IPA can be quite large, with magnitudes exceeding the plane-parallel bias of about 0.1 and in one area even exceeding 0.3. However, the horizontal average of the IPA bias is an order of magnitude smaller than the plane-parallel bias, because the positive and negative regions tend to approximately cancel in the area average.

The IPA has a long history of use in remote sensing, and was employed in a theoretical study by Ronnholm et al. (1980). But without any explicit model of the spatial structure, previous studies could not examine the errors in the IPA. Here we find significant local errors in the IPA fluxes for the 2D bounded cascade, even though this model does not include geometrical cloud effects. We emphasize that the IPA is justified for this model only for the mesoscale-average reflected flux, and even

this breaks down for a singular cascade (Cahalan (1989), Cahalan et al. (1994b)).

When the sun is closer to the zenith than $\theta_o = 60°$, the IPA errors tend to be of the same sign, but much smaller in magnitude, since most of the photons are scattered in the forward direction. On the other hand, when the sun approaches the horizon, the reflectivity everywhere approaches 1, so all the biases are again smaller than at $\theta_o = 60°$. As a result, the total IPA bias is maximum when the sun is near 60° (Cahalan et al., 1994.)

Since the horizontal average of the IPA errors is quite small for the bounded cascade, we may employ the IPA to estimate the average albedo, and compare it with the albedo of a uniform cloud having the same horizontal average optical depth. Thus we substitute this difference for the "plane-parallel albedo bias" defined in Eq. (1). It can be shown that the resulting plane-parallel bias is strictly positive as long as the reflection function is convex, unlike the IPA errors. (See for example Jensen, 1906.) The plane-parallel albedo for the parameters used here is 0.69, while the average of Monte Carlo albedo (i.e. averaging over a number of realizations such as that in Fig. 2a) is about 0.6. Thus the bias associated with using the area-average optical thickness is about 0.09, or 13% of the plane-parallel albedo. [Note that the bias is always underestimated by taking only a finite number of cascades.]

As a result of the IPA, the mean albedo may be computed by simply transforming the liquid water (or optical depth) of each pixel to reflectivity, and then averaging over all pixels. The results in the case of conservative scattering are shown in Fig. 3. The upper curve is the plane-parallel ($f = 0$) albedo as a function of mean liquid water path, and the lower curve is the fractal ($f = 0.5$) albedo. For a typical mean liquid water path of $W \approx 100$ g/m^2 ($\tau_v \approx 15$), Fig. 3 shows that the plane-parallel albedo of about 0.69 is reduced to about 0.60 by the fractal structure, implying a relative bias of approximately 15%. In order to obtain the correct albedo from a plane-parallel cloud, it is necessary to reduce the liquid water path, or optical thickness, by 30%. An explicit expression for this reduction is derived in Section 5.

Since the reflectivity of a given pixel is a function of the local liquid water path, it may be expanded in a Taylor series as follows:

$$R(W) = R(\overline{W}) + (W - \overline{W})R^{(1)}(\overline{W}) + \frac{1}{2}(W - \overline{W})^2 R^{(2)}(\overline{W}) + \cdots , \quad (4)$$

where $\overline{W}$ is the average liquid water path, and $R^{(n)}(\overline{W})$ is the nth derivative of R wrt W, evaluated at $\overline{W}$. [We have supressed the dependence of R on the solar zenith angle.] Averaging both sides of Eq. (4) then gives

$$\overline{R(W)} = R(\overline{W}) + \frac{1}{2}\mu_2 R^{(2)}(\overline{W}) + O(\mu_3 R^{(3)}) , \quad (5)$$

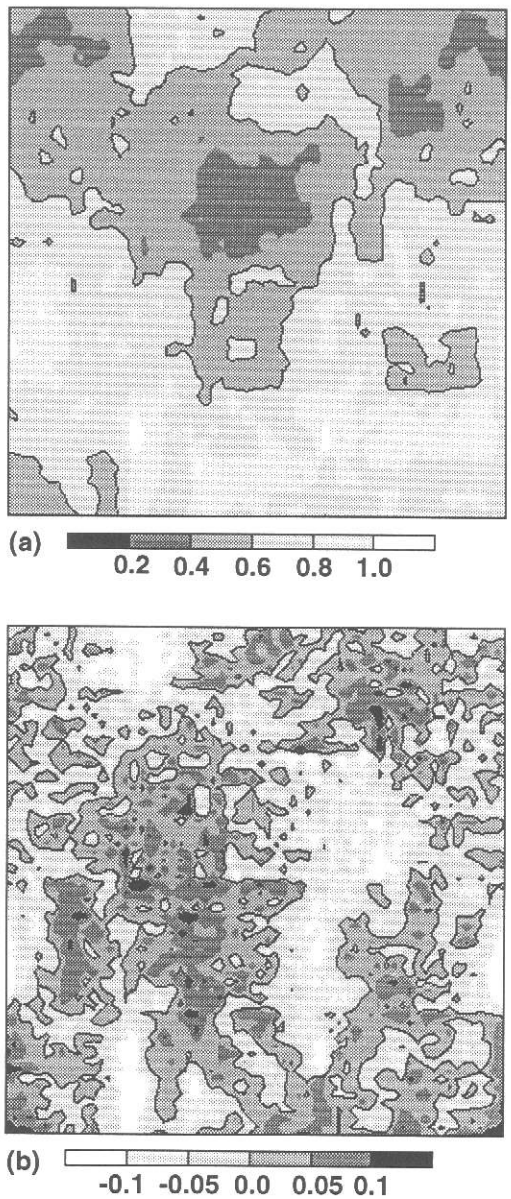

Fig. 2. (a) Reflectance as a function of position in a bounded cascade cloud with $A_c = 1$ and $f = 0.5$. Starting with a uniform cloud having mean vertical optical thickness $\overline{\tau} = \tau_v = 16$, 6 cascades were generated in each horizontal direction, giving $2^{12} = 4096$ uniform elements or "pixels". Reflectivities were computed by Monte Carlo with 10^7 photons. Microphysical properties are uniform, with single-scattering albedo $\omega_o = 1$ and asymmetry $g = 0.85$. The Henyey-Greenstein phase function was used, but essentially identical results were obtained with the "fair weather cumulus" function. The sun is 60° to the left of vertical. The black contour at 0.6 shows approximately where the reflectance equals the mean reflectance, with more reflective regions lighter, and less reflective regions darker. (b) The "independent pixel bias", defined as the independent pixel reflectances (computed from the vertical optical thickness of each pixel) minus the Monte Carlo reflectances shown in (a). While the local biases range from 0.257 to -0.302, the area-average is 0.0096, nearly an order of magnitude smaller than the "plane-parallel bias", namely the reflectance of the mean optical thickness minus the mean of the independent pixel reflectances, which is about 0.08.

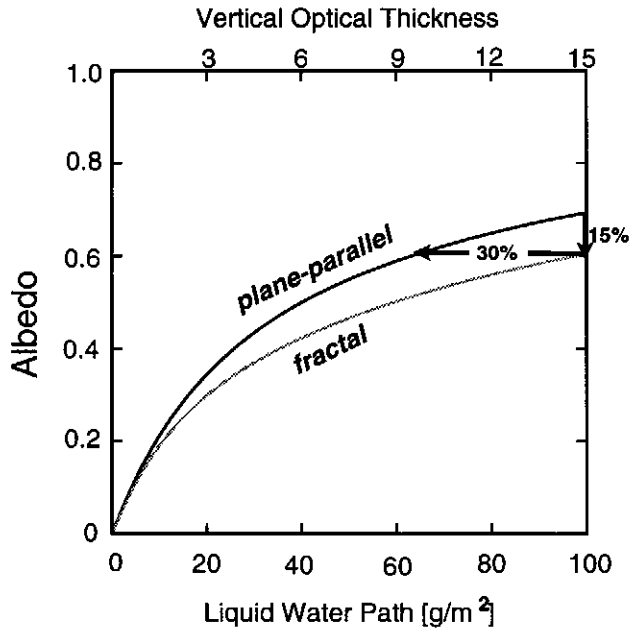

Fig. 3. Dependence of albedo on mean liquid water path and vertical optical thickness for the two approaches shown in Figs. 1a and 1c, where the fractal case (c) is computed from the bounded model for $A_c = 1$ and $f = 0.5$, using the independent pixel approximation. Subtracting the mean reflectance (the lower curve) from the reflectance of the mean (the upper curve) gives the "plane-parallel bias". When $\tau_v = 15$ the bias is 15% of the plane-parallel albedo, and the mean reflectance equals that of a plane-parallel cloud with 30% less liquid water, or an optical thickness $\tau_{eff} = 10$.

where μ_2 is the second moment, or variance, of the one-point distribution of W generated by the bounded cascade. Subtracting Eq. 5 from $R(\overline{W})$ gives the plane-parallel albedo bias. The lowest-order term is positive, since $R^{(2)}$ is negative. This term overestimates the bias, while inclusion of the μ_3 term underestimates, and so on (see Cahalan et al. (1994a)). Appendix A shows that all the moments of the bounded model may be obtained from μ_2 as a function of f, thus formally determining all the coefficients in the above expansion. In Section 5 we consider an alternative expansion about $\overline{\log(W)}$, which leads to a simple expression for the effective liquid water path and effective thickness. First, however, we briefly review the dependence of the bias on cloud fraction, A_c, to show that the case of $A_c = 1$, assumed in the above discussion, produces the largest plane-parallel albedo bias during the diurnal cycle of California marine stratocumulus.

4 Diurnal cycle

The total plane-parallel albedo bias has two contributions, as described in Eq. (2): that due only to cloud fraction, which is given by Fig. 1a minus Fig. 1b, and that due to the fractal structure, given by Fig. 1b minus Fig. 1c. The fractal structure contribution is largest when the liquid water variance is largest, which in the case of California marine stratocumulus occurs during the morning hours, when the cloud fraction is nearly 100%, as shown in Cahalan et al. (1994a). Although the cloud fraction contribution to the bias is larger in the afternoon, when the cloud fraction drops to 60%, this is more than offset by the decrease in the liquid water variance, which reduces both the fractal contribution and the total bias. The fact that the cloud variance is largest when the cloud cover is largest leads to the surprising result that plane-parallel estimates are most in error when the usual "cloud-fraction" corrections vanish!

In Cahalan et al. (1994a) the diurnal cycle of the albedo bias was estimated indirectly, by first computing the diurnal cycle of f, determined from hourly values of the variance of $\log(W)$. Here we compute the bias directly from the time series of W, by performing a plane-parallel computation of reflectance for each observation, and then compositing the results hourly. The direct results agree qualititatively with the earlier indirect approach, and are shown in Fig. 4, which is qualitatively similar to Fig. 9 in Cahalan et al. (1994a). Here the lower curve is the usual correction due only to cloud fraction, and vanishes when the fraction reaches 100%; the middle curve is the additional correction due to the fractal distribution of the cloud liquid water; and the upper curve is the total albedo bias. Note that the cloud fraction correction is much smaller than the total, is 180° out of phase with the total during most of the day, except when the sun is setting, when the total is dominated by the cloud fraction correction due to the neglect of the clear-sky albedo. The 0.09 albedo reduction needed when the clouds are overcast represents a major change in the average cloud albedo of 0.6.

5 Effective optical thickness

Since the largest albedo bias occurs for overcast cloudiness conditions, when $A_c = 1$, let us further consider that case, represented by the 15% increase in Fig. 3 of the albedo of a plane-parallel cloud over that of a fractal with the same total cloud water. As shown in Cahalan et al. (1994a), this bias may be estimated from a simple "effective thickness approximation", which is a lowest-order approximation to the bias determined from the IPA. To derive it, consider an expansion similar to Eq. (4), except now the local reflectance is considered as a function of the *logarithm* of the local liquid water path, $\log(W)$, and expanded in a Taylor series about the mean, $\overline{\log(W)}$. Taking the mean of the result gives the mean cloud reflectivity as:

$$\overline{R(\log(W))} = R(\overline{\log(W)}) + \frac{1}{2} M_2 R''(\overline{\log(W)}) + O(M_4 R''''), \quad (6)$$

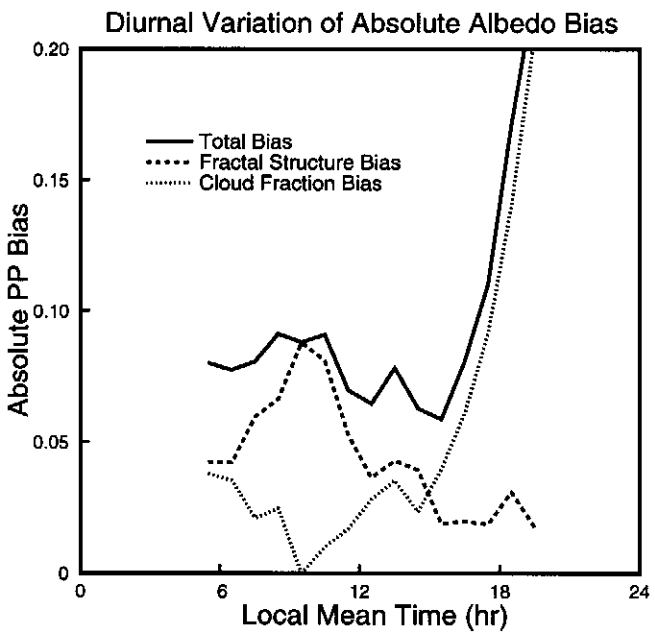

Fig. 4. Absolute plane-parallel albedo bias as a function of time-of-day for California marine stratocumulus, determined directly from microwave measurements of liquid water path during 18 days in June 1987, by computing an independent reflectivity from each measurement. The same computation using the bounded cascade model with diurnally varying f and A_c is given in Cahalan et al. (1994a), and is qualitatively similar. The upper solid curve is the total bias defined as in Eq. (1), while the dotted and dashed curves are the contributions due to cloud fraction and fractal structure, respectively, as defined in Eq. (2). Cloud fraction is defined as the fraction of values exceeding 10 g/m^2, and clear-sky albedo is taken to be zero.

where M_2 is the variance of $\log(W)$, given in Appendix B, and R'' is the second derivative of R wrt $\log(W)$ evaluated at the mean of $\log(W)$. It can be shown that the odd moments vanish in the bounded cascade, so that only the even moments appear in Eq. (6). As a function of $\log(W)$, the conservative reflection function has an inflection point, where the slope ceases increasing with $\log(W)$ and begins to decrease, and the curvature vanishes. This typically occurs near $\overline{\log(W)}$. Thus the second term in the preceeding equation is small, so that the mean reflectivity is approximately given by the reflectivity evaluated at $\overline{\log(W)}$. In the bounded cascade model, the mean of $\log(W)$ is given by

$$\overline{\log(W)} = \log(W_{eff}), \tag{7}$$

where the "effective liquid water path" is

$$W_{eff} = \overline{W} * \chi(f, c), \tag{8}$$

and $\chi(f, c) < 1$ is the "reduction factor" given in Eq. (B2), and is approximately 0.7 when $f = 0.5$ and $c = 0.8$.

Combining Eqs. (8) and (3) allows us to define the "effective optical thickness" as

$$\tau_{eff} = \tau_v * \chi(f, c), \tag{9}$$

where τ_v is the mean vertical optical thickness. Taking only the first term in the expansion in Eq. (6), and using Eq. (3), it is clear that for a range of intermediate mean cloud thicknesses near the inflection point of the reflectivity, the mean albedo may be approximated by the plane-parallel albedo evaluated at the effective thickness, as follows:

$$\overline{R(\tau)} \approx R(\tau_{eff}), \tag{10}$$

An estimate of the plane-parallel albedo bias may be obtained by simply subtracting Eq. (10) from the plane-parallel albedo, $R(\tau_v)$. The relative error in the estimate of the bias derived from Eq. (10) is shown in Fig. 5 as a function of f and τ_v, for $c = 0.8$ and a solar zenith angle of $\theta_o = 60°$, which is typical for subtropical stratocumulus. For the contours labelled ± 30, for example, the bias obtained from the simple effective thickness approximation should be multiplied by 1 ∓ 0.3. Since the bias itself is on the order of 0.1, this corresponds to corrections of $\approx \mp 0.03$. The correction is dominated by the M_2 term in Eq. (6), and thus changes sign near the inflection point of $R(\log(W))$.

According to (9), the effective thickness depends on the fractal structure through χ, which is a known analytic function of the fractal parameters f and c. The fractal parameter f is in turn adjusted to give the observed value of σ, a known analytic function of f and c, while c is fixed by the exponent of the wavenumber spectrum. Thus τ_{eff} is parametrically determined

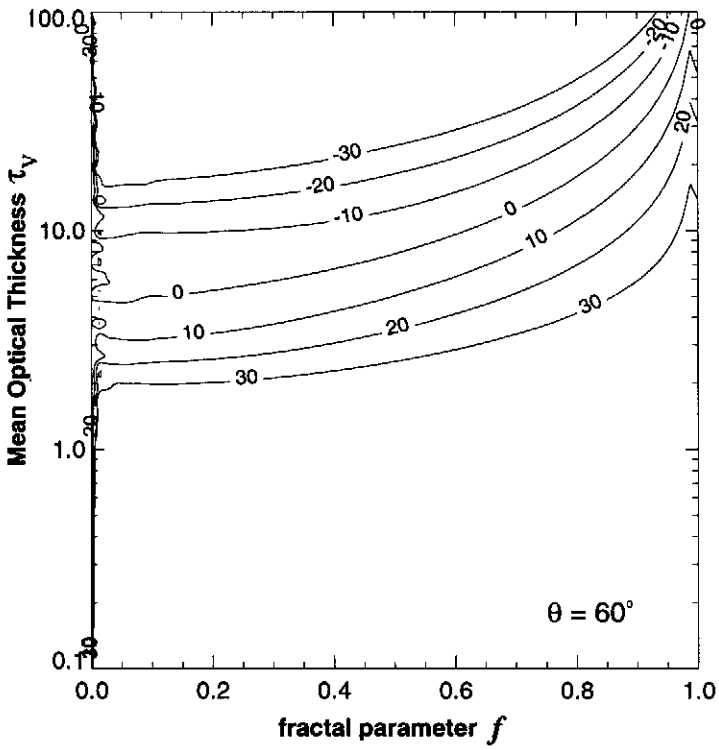

Fig. 5. Relative error in percent in the plane-parallel bias when the actual albedo is approximated by the plane-parallel albedo at a reduced "effective thickness", as a function of mean optical thickness τ_v and fractal parameter f. If the effective thickness gives an absolute bias of 0.10 near the -20 contour, for example, then the actual bias should be *increased* 20%, to 0.12, and similarly an estimate of 0.10 near the +20 contour should be *decreased* to 0.09. These same corrections also apply to the relative bias.

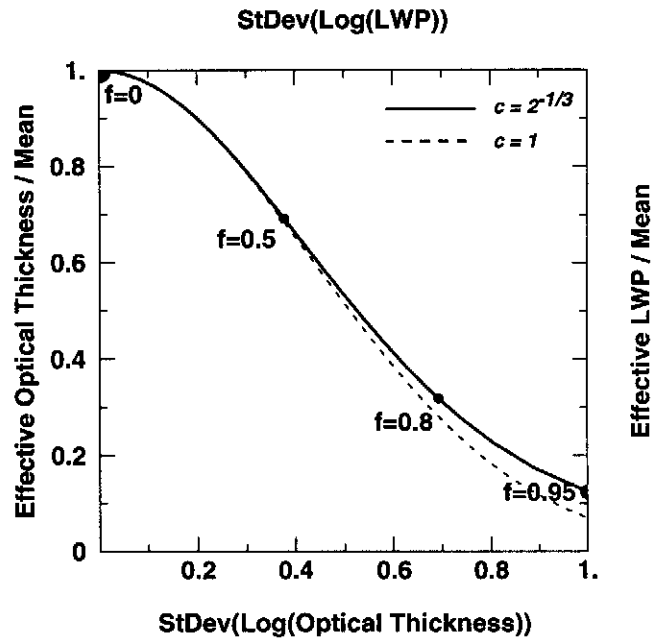

Fig. 6. Plot of χ, the reduction factor, versus σ, the standard deviation of $\log_{10}(W)$. Both the horizontal and vertical scales are scale-invariant, and apply to either W or τ because of the simple linear relation expressed in Eq. (3). The solid curve is for the bounded model with $c \approx 0.8$, while the dashed curve is the singular limit given by the simple expression in Eq. (B11). Labelled points apply only to the upper curve. The value of σ derived from observations of California marine stratocumulus is 0.39, corresponding to $\chi \approx 0.7$, which occurs at $f = 0.5$. (This is the diurnal mean in the summer, when f varies from about 0.6 in the morning to 0.3 in the afternoon.) The global reduction factor $\chi \approx \frac{1}{3}$ discussed by Harshvardhan and Randall (1985) occurs at $f = 0.8$, and requires a global value of $\sigma \approx 0.7$.

as a function of σ by varying f. Details are given in Appendix B, and results are shown in Fig. 6 for both $c = 2^{-1/3} \approx 0.8$ needed to give a 5/3 wavenumber spectrum, and for the singular limit $c \to 1$, for which χ is a simple exponential given in Eq. (B11). The point labelled $f = 0.5$ corresponds to the diurnal average value of $\sigma = 0.39$ determined from the stratocumulus observations discussed in Section 4. In this case $\chi \approx 0.7$, so for example when $\tau_v = 15$ we have $\tau_{eff} \approx 10$, and $\overline{R} \approx 0.6$.

Harshvardhan and Randall suggested that the global average cloud liquid must be reduced by a factor of approximately 0.3 in order to obtain the correct global albedo. To obtain this value of the reduction factor, $\chi = 0.3$, in the current model requires an increase in the fractal parameter to $f = 0.8$, and an increase in the standard deviation to $\sigma = 0.7$, as seen in Fig. 6. This in turn increases the plane-parallel albedo bias by a factor of 5. The fact that a much larger bias is found on a global basis is presumably due to the much wider variation in cloudiness over the globe, as compared to the relatively benign variation in marine stratocumulus. Davis et al. (1990) considered a related quantity, the "packing factor", the inverse of the reduction factor,

and studied the thick cloud limit in a singular model, for which $\chi \to 0$, and the packing factor diverges. A similar singular model was studied in Cahalan, 1989. The bounded model considered here is a relatively conservative extension of the plane-parallel idealization. More radical, and perhaps singular, models may be needed to better represent radiative processes in deep convective cloud systems.

6 Conclusions

This paper has extended previous results on the average albedo of bounded cascade clouds, with parameters appropriate for marine stratocumulus clouds, known to be a major contributor to cloud radiative forcing. The model reproduces the observed power spectrum and low-order moments of the liquid water distribution in marine stratocumulus, and was studied here by both Monte Carlo and analytic methods. Previous results for the dependence of local fluxes on horizontal photon transports were extended from 1D cascades to 2D cascades in Sect. 3, showing that errors in estimates of local fluxes from the "independent pixel approximation" (IPA) can be large in some regions, while still producing an area-average reflectivity which is accurate to about 1% for a 2D bounded cascade. Previous results for the diurnal variation in the albedo bias were reproduced directly from the observations without using the cascade model, as discussed in Sect. 4, verifying again that the bias is largest for 100% cloud fraction. These results suggested a way of parameterizing the impact of cloud variability on the large-scale albedo in terms of an "effective liquid water path", W_{eff} (or equivalently an "effective optical thickness", τ_{eff}), smaller than the mean by a factor which depends only on the fractal structure. Section 5 determined the accuracy of this "effective thickness approximation" (ETA) as a function of the fractal parameter f and the mean liquid water path, $\overline{W}$ (or equivalently the mean optical thickness, τ_v). The ratio of $\chi = W_{eff}/\overline{W}$ (or τ_{eff}/τ_v) was determined as an analytic function of the fractal parameters, and as a parametric function of σ, the standard deviation of $\log_{10}(W)$ (or $\log_{10}(\tau)$), which may be estimated directly from observations.

For marine stratocumulus, $\sigma \approx 0.4$ and $\chi \approx 0.7$, so that the mean albedo equals that of a plane-parallel cloud having 30% less liquid water, which is approximately 15% less than that of a plane-parallel cloud having an equal amount of liquid water. The plane-parallel albedo requires the largest adjustment when the cloud fraction is nearly 100%, since that is when the largest variability is observed. Thus the largest correction occurs when the usual cloud fraction correction is small.

The bounded cascade model studied here represents an extension to plane-parallel clouds which is relatively conservative, since the cloud height and base are fixed, the microphysics is uniform, and the variability of cloud optical properties is relatively mild. Yet even this conservative model shows that the variability of liquid water in marine stratocumulus can have a larger impact on the mesoscale average albedo than the usual cloud fraction corrections. For cloud types not confined to a single vertical layer, such as those found in deep convective regions, geometrical fractal properties neglected here may also impact large-scale radiative properties, and may well require more radical departures from conventional plane-parallel ideas. Further study of the structure and radiation of real clouds in their full complexity will be needed in order to understand how Earth's climate is being regulated, and in order to consistently quantify the role played by Earth's cloud systems on the energy and hydrological cycles.

Appendix A Rescaling f generates W moments

Here we derive expressions for the moments about the origin of the liquid water path generated by a bounded cascade, as a function of the cascade parameters f and c. We show that all moments may all be obtained from the second moment considered as a function of f, by rescaling the values of f. This generalizes low-order results derived in Appendix B of Cahalan et al. (1994a), and shows in particular that all moments approach those of a lognormal in the singular limit $c \to 1$.

It is convenient to first define two sets of nth-order polynomials:

$$P_n(x) \equiv \frac{\left(1+\sqrt{x}\right)^{2n} + \left(1-\sqrt{x}\right)^{2n}}{2} = \sum_{m=0}^{n} \binom{2n}{2m} x^m, \tag{A1}$$

and

$$Q_n(x) \equiv \frac{\left(1+\sqrt{x}\right)^{2n+1} + \left(1-\sqrt{x}\right)^{2n+1}}{2} = \sum_{m=0}^{n} \binom{2n+1}{2m} x^m. \tag{A2}$$

For example, the first three are given by:

$P_n(x)$	$Q_n(x)$
$1+x$	$1+3x$
$1+6x+x^2$	$1+10x+5x^2$
$1+15x+15x^2+x^3$	$1+21x+35x^2+7x^3$

for $n = 1, 2, 3$.

Values of liquid water in the bounded cascade have the form

$$W = \prod_{k=0}^{\infty} \left(1 \pm f\, c^k\right), \tag{A3}$$

where f,$c \in (0,1]$. After averaging over $\pm$, the moments depend only on $a = f^2$ and $s = c^2$, and can be written in terms of the above polynomials in the form:

$$\mu_{2n}(a,s) = \prod_{k=0}^{\infty} P_n\left(as^k\right), \tag{A4}$$

and

$$\mu_{2n+1}(a,s) = \prod_{k=0}^{\infty} Q_n\left(as^k\right). \tag{A5}$$

For example, when $n = 1$,

$$\mu_2(a,s) = \prod_{k=0}^{\infty}\left(1+as^k\right) = 1+\sum_{m=1}^{\infty}\left(\frac{s^{m(m+1)/2}}{\prod_{k=1}^{m}\left(1-s^k\right)}\right)a^m, \tag{A6}$$

and

$$\mu_3(a,s) = \prod_{k=0}^{\infty}\left(1+3as^k\right) = \mu_2(3a,s). \tag{A7}$$

The last expression for μ_2 in Eq. (A6) was originally derived by Euler, as discussed for example in Hardy and Wright (1979, p.280). Taking the limit $s \to 1$, we can use the fact that $\lim_{s\to 1}\frac{1-s^k}{1-s} = k$ to show that

$$\lim_{s\to 1}\left(\frac{\mu_2}{\exp\left(\frac{a}{1-s}\right)}\right) = 1, \tag{A8}$$

which implies an essential singularity in μ_2. The third moment is also singular, since

$$\lim_{s\to 1}\left(\frac{\mu_3}{(\mu_2)^3}\right) = 1. \tag{A9}$$

We now generalize Eqs. (A7) and (A9) to the remaining moments. By application of Sturm's theorem, it can be shown that the roots of P_n,Q_n all lie on the negative real axis, so that we may write:

$$P_n(x) = \prod_{i=1}^{n}\left(1+R_i^{(n)}x\right), \tag{A10}$$

and

$$Q_n(x) = \prod_{i=1}^{n}\left(1+\tilde{R}_i^{(n)}x\right) \tag{A11}$$

where the $R^{(n)}$,$\tilde{R}^{(n)}$ are sets of positive real numbers with n elements. The first three sets are:

$R^{(n)}$	$\tilde{R}^{(n)}$
1	3
$3-\sqrt{8}, 3+\sqrt{8}$	$5-\sqrt{20}, 5+\sqrt{20}$
$7-\sqrt{48}, 1, 7+\sqrt{48}$	$0.232, 1.572, 19.196$

Moments $2n$ and $2n+1$ thus factor into n infinite products:

$$\mu_{2n}(a,s) = \prod_{i=1}^{n}\mu_2\left(R_i^{(n)}a,s\right), \tag{A12}$$

and

$$\mu_{2n+1}(a,s) = \prod_{i=1}^{n}\mu_2\left(\tilde{R}_i^{(n)}a,s\right), \tag{A13}$$

so that all moments are determined by products of the second moment evaluated at various rescaled values of the fractal parameter $a = f^2$. Combining Eqs. (A8) and (A12), we find that in the singular limit,

$$\lim_{s\to 1}\left(\frac{\mu_{2n}}{(\mu_2)^{\sum_{i=1}^{n}R_i^{(n)}}}\right) = 1, \tag{A14}$$

with a similar expression for the odd moments with $R_i \to \tilde{R}_i$. The sum of the roots can be shown to equal the coefficient of the linear term in Eq. (A1), so that:

$$\sum_{i=1}^{n}R_i^{(n)} = 2n(2n-1)/2, \tag{A15}$$

and similarly for $\tilde{R}_i$. The limits for the even and odd moments can then be combined to yield:

$$\lim_{s\to 1}\left(\frac{\mu_n}{(\mu_2)^{n(n-1)/2}}\right) = 1, \tag{A16}$$

consistent with the behavior of moments of a lognormal.

Appendix B W_{eff}, χ, and σ

Here we derive polynomial expansions for the reduction factor, $\chi \equiv W_{eff}/\overline{W}$, and $\sigma \equiv$ standard deviation of $\log_{10}(W)$ = standard deviation of $\log_{10}(\tau)$, as a function of the fractal parameter f, with coefficients depending on c. In the case $c = 2^{-1/3}$, needed for a 5/3 spectral exponent, we provide accurate rational functions of f for $\log_{10}(\chi)$ and σ. Finally, an approximate expression for $\chi(\sigma)$ is determined.

The "effective optical thickness" defined in Section 5 is based on the following result for the liquid water path, W:

$$\overline{\log(W)} = \log(\chi\,\overline{W}), \tag{B1}$$

where the overbar signifies an area average and an ensemble average, and where the "reduction factor" is given by

$$\chi(f,c) = \left(\prod_{n=0}^{\infty}\left(1-f^2c^{2n}\right)\right)^{\frac{1}{2}}. \tag{B2}$$

Here f varies diurnally, as discussed in Sect. 4, but c is assumed constant, given by $c = 2^{-\frac{1}{3}}$, or

$$c^2 = 0.630, \tag{B3}$$

as required for a $k^{-\frac{5}{3}}$ wavenumber spectrum. Equation B2 was derived in Cahalan et al. (1994a) from the statistical distribution generated by the bounded cascade model. The reduction factor may also be expressed as

$$\chi(f,c) = 10^{-\Delta(f,c)}, \tag{B4}$$

where

$$\Delta(f,c) \equiv \log_{10}(\overline{W}) - \overline{\log_{10}(W)}, \tag{B5}$$

A polynomial expression for Δ is obtained by taking $\log_{10}$ of Eq. (B2) and expanding in a power series in f, leading to

$$\Delta(f,c) = \frac{\log_{10}(e)}{2}\frac{f^2}{1-c^2}\left(1 + \frac{f^2}{1+c^2} + O\left(f^4\right)\right) \tag{B6}$$

For the value of c^2 given in Eq. (B3), a better fit than Eq. (B6) is given by the rational function:

$$\Delta(f) = 0.594\, f^2 \left(\frac{1 - 0.485 f^2}{1 - 0.739 f^2}\right), \tag{B7}$$

which is accurate to 1% as long as $f < 0.9$.

The second moment of $\log_{10}(W)$ was derived in Cahalan et al. (1994a), and is given by

$$M_2(f,c) = \sum_{k=0}^{\infty}\left(\frac{1}{2}\log_{10}\left(\frac{1+fc^k}{1-fc^k}\right)\right)^2 \tag{B8}$$

If we take the square root of Eq. (B8), and expand the result in powers of f, we obtain the standard deviation of $\log_{10}(W)$ in the form:

$$\sigma(f,c) = \frac{f\log_{10}(e)}{\sqrt{1-c^2}}\left(1 + \frac{1}{3}\frac{f^2}{1+c^2} + O\left(f^4\right)\right). \tag{B9}$$

The first term here agrees with the standard deviation obtained by taking the square root of the exponent of μ_2 in the singular limit in Eq. (A8). For the value of c^2 in Eq. (B3) a better fit is given by the rational function:

$$\sigma(f) = 0.718\, f \left(\frac{1 - 0.556 f^2}{1 - 0.729 f^2}\right). \tag{B10}$$

which is accurate to 1% as long as $f < 0.9$.

Solving for f in Eq. (B9), and substituting the result in Eq. (B6) allows us to write Eq. (B4) to lowest order as:

$$\chi(\sigma) \approx 10^{-\sigma^2/(2\log_{10}(e))} \approx 10^{-1.15\sigma^2}. \tag{B11}$$

The leading term in the exponent in Eq. (B11) is independent of c, and the correction terms are of order σ^4, and do not become important until $\sigma > 0.5$ or so. This can be seen in Fig.6, where the exact $\chi(\sigma)$ in the case that c is given by Eq. (B3) is plotted along with Eq. (B11). In the singular limit $c \to 1$, the upper solid curve moves down toward the dashed one. Since σ diverges for any fixed value of f (from Eq. (B9) the labelled points all slide down toward the right as c increases, so that χ approaches zero for any fixed f.

Acknowledgements. The author thanks T. Bell, Harshvardhan, M. King, W. Rossow, G. Stephens, B. Wielicki and W. Wiscombe for discussions on climatic effects of fractal cloud structure, A. McConnell and H. Rubin for discussions on the moment problem, and W. Ridgway and D. Silberstein for carrying out a number of numerical computations.

References

Cahalan, R. F., Overview of fractal clouds, Advances in Remote Sensing, A. Deepak Publishing, 515+pp, pp. 371–388, 1989.

Cahalan, R. F. and J. B. Snider, Marine stratocumulus structure, *Remote Sens. Environ.*, *28*, 95–107, 1989.

Cahalan, R. F. and W. J. Wiscombe, Impact of cloud structure on climate, Current Problems in Atmospheric Radiation, A. Deepak Publishing, 565+pp, pp. 120–124, 1993.

Cahalan, R. F., W. Ridgway, W. J. Wiscombe, T. L. Bell and J. B. Snider, 1994: The albedo of fractal stratocumulus clouds, *J. Atmos. Sci.* **51**, 1994.

Cahalan, R. F., W. Ridgway, W. J. Wiscombe, S. Gollmer and Harshvardhan, Independent pixel and Monte Carlo estimates of stratocumulus albedo, to appear in *J. Atmos. Sci.*, 1994.

Davis, A., P. Gabriel, S. Lovejoy, D. Schertzer and G. Austin, Discrete angle radiative transfer III: numerical results and meteorological applications, *J. Geophys. Res.* **95**, 11,729–11,742, 1990.

Gabriel, P., S. Lovejoy, A. Davis, D. Schertzer and G. Austin, Discrete angle radiative transfer II: renormalization approach for homogeneous and fractal clouds, *J. Geophys. Res.* **95**, 11,717–11,728, 1990.

Hardy, G. H. and E. M. Wright, *An Introduction to the Theory of Numbers*, Oxford Science Publications, Fifth Edition, Oxford University Press, 426pp., c1979.

Harshvardhan and D. Randall, Comments on "the parameterization of radiation for numerical weather prediction and climate models," *Mon. Wea. Rev.* **113**, 1832–1833, 1985.

Jensen, J. L. W. V., Sur les fonctions convexes et les inégalitiés entre les valeurs moyennes, *Acta Math.* **30**, 175–193, 1906.

Lovejoy, S., A. Davis, P. Gabriel, D. Schertzer and G. Austin, Discrete angle radiative transfer I: scaling and similarity, universality and diffusion, *J. Geophys. Res.* **95**, 11,699–11,715, 1990.

Marshak, A., A. Davis, R. F. Cahalan, and W. J. Wiscombe, Bounded cascade models as non-stationary multifractals, *Phys. Rev. E* **49**, 55–69, 1994.

Ramanathan, V., R.D. Cess, E.F. Harrison, P. Minnis, B. R. Barkstrom, E. Ahmad and D. Hartmann, Cloud-radiative forcing and climate: results from the Earth-radiation Budget Experiment", *Science* **243**, 57–63, 1989.

Ronnholm, K., M. B. Baker and H. Harrison, Radiative transfer through media with uncertain or variable parameters, *J. Atmos. Sci.* **37**, 1279–1290, 1980.

Stephens, G. L., Reply (to Harshvardhan and Randall), *Mon. Wea. Rev.* **113**, 1834–1835, 1985.

Sundqvist, H., E. Berge and J. E. Kristjansson, Condensation and cloud parameterization studies with a mesoscale numerical weather prediction model, *Mon. Wea. Rev.* **117**, 1641–1657, 1989.